Korea-Australia Rheology Journal
Vol. 19, No. 4, December 2007 pp. 233-242

Finite element analysis of elastic solid/Stokes flow interaction problem

Jin Suk Myung, Wook Ryol Hwang[1,*], Ho Youn Won[2], Kyung Hyun Ahn, and Seung Jong Lee
School of Chemical and Biological Engineering, Seoul National University, Seoul 151-744, Korea
[1] School of Mechanical and Aerospace Engineering, Research Center for Aircraft Parts Technology (ReCAPT), Gyeongsang National University, Jinju 660-701, Korea
[2] Hanwha Chemical, Research and Development Center, Daejeon 305-804, Korea
(Received July 20, 2007, final revision received November 28, 2007)

Abstract

We performed a numerical investigation to find out the optimal choice of the spatial discretization in the distributed-Lagrangian-multiplier/fictitious-domain (DLM/FD) method for the solid/fluid interaction problem. The elastic solid bar attached on the bottom in a pressure-driven channel flow of a Newtonian fluid was selected as a model problem. Our formulation is based on the scheme of Yu (2005) for the interaction between flexible bodies and fluid. A fixed regular rectangular discretization was applied for the description of solid and fluid domain by using the fictitious domain concept. The hydrodynamic interaction between solid and fluid was treated implicitly by the distributed Lagrangian multiplier method. Considering a simplified problem of the Stokes flow and the linearized elasticity, two numerical factors were investigated to clarify their effects and to find the optimum condition: the distribution of Lagrangian multipliers and the solid/fluid interfacial condition. The robustness of this method was verified through the mesh convergence and a pseudo-time step test. We found that the fluid stress in a fictitious solid domain can be neglected and that the Lagrangian multipliers are better to be applied on the entire solid domain. These results will be used to extend our study to systems of elastic particle in the Stokes flow, and of particles in the viscoelastic fluid.

Keywords : finite element method, fictitious domain, Lagrangian multiplier, solid/fluid interaction

1. Introduction

The solid/fluid interaction problem is one of remaining challenges in the numerical simulation of particle-filled fluids. There are several methods available for the simulation of particle systems: *e.g.*, the Brownian dynamics (Allen and Tildesley, 1987; Hütter, 1999), meso-scale particle simulations (Trofimov, 2003), micro-macro simulations, and direct numerical simulations (DNS). Each method has its own pros and cons. For example, the Brownian dynamics is not practical in solving the flow field with many-body hydrodynamics; the meso-scale particle simulation such as the lattice-Boltzmann method, the dissipative particle dynamics, and the fluid particle dynamics make implicit assumptions for the potentials involved in the system; the micro-macro simulation which is based on the CONNFFESSIT (Calculation of Non-Newtonian Flow: Finite Element and Stochastic Simulation Technique) algorithm (Laso and Öttinger, 1993) requires a large number of particles with random noises. Our long-term objective is to understand dynamics of deformable particles in complex flow fields with high precision. To take the full hydrodynamic interaction into account, the direct numerical simulation method has the advantage over the others since it is possible to get the velocity field near the particle, and moreover the constitutive models for both solid and fluid can be easily combined (Hwang *et al.*, 2004).

For solid/fluid interaction problems, both Lagrangian and Eulerian methods are widely used. The Lagrangian approach, *e.g.* Doner et al. (1981) or Hu (1996), usually needs frequent remeshing and the projection of solutions and its usage is seriously limited in 3D simulations due to difficulty in remeshing in solid/liquid flow. Using the fictitious domain method, one can avoid remeshing and solve the problem with a simple regular mesh, which is especially beneficial in 3D simulation. In this study, the fictitious domain method will be used with which constraints on the solid boundary (*or* over the solid domain) are represented by the distributed Lagrangian multipliers (Glowinski *et al.*, 1999). The overview of the distributed-Lagrangian-multiplier/fictitious-domain (DLM/FD) method is well documented in Glowinski *et al.* (1999), Baaijens (2001), and Yu (2005).

In this study, we apply the distributed-Lagrangian-mul-

*Corresponding author: wrhwang@gsnu.ac.kr

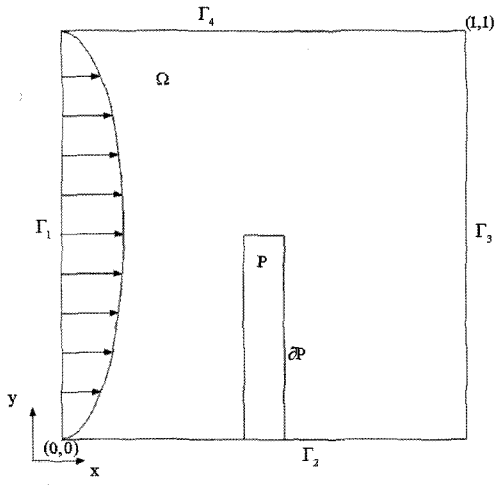

Fig. 1. Schematic diagram of the model problem: an elastic solid bar is attached on the bottom in a pressure-driven channel flow.

tiplier/fictitious-domain (DLM/FD) method to a simple elastic solid/Stokes flow interaction problem. We investigate the effect of the distribution of the Lagrangian multipliers and the effect of interfacial conditions between the fluid and solid meshes. A simple model problem is constructed such that an elastic bar attached on the bottom of the wall is subjected to a pressure-driven channel flow. The results from this study will be helpful in extending our work to the system of a suspended elastic particle in a fluid or in a viscoelastic fluid.

The paper is structured as follows. In section 2, we introduce the problem definition and governing equations. In section 3 the numerical methods and conditions are explained. In section 4 we describe implementation techniques. Then in section 5 we show the numerical results on the mesh convergence, the pseudo-time step dependence, the solid/fluid mesh ratio, etc. Finally we summarize the results with some conclusions.

2. Governing sets of equations

As presented in Fig. 1, we consider an elastic solid bar attached on the bottom under the pressure-driven channel flow of a Newtonian fluid. The computational domain is denoted by Ω, and its boundary is denoted by Γ. The symbols P and ∂P represent the solid domain and its boundary, respectively.

2.1. Fluid domain

The set of equations in the fluid domain is simply of the Stokes flow:

$$\nabla \cdot \boldsymbol{\sigma}_f = 0 \quad \text{in } (\Omega \backslash P), \tag{1}$$

$$\nabla \cdot \boldsymbol{v}_f = 0 \quad \text{in } (\Omega \backslash P), \tag{2}$$

$$\boldsymbol{\sigma}_f = -p_f \boldsymbol{I} + 2\eta \boldsymbol{D}(\boldsymbol{v}_f) \quad \text{in } (\Omega \backslash P). \tag{3}$$

Eqs. (1)-(3) are for the momentum balance, the continuity, and the constitutive relation, respectively, in the fluid domain. The symbols $\boldsymbol{\sigma}_f$, $\boldsymbol{v}_f$, p_f, $\boldsymbol{I}$, η and $\boldsymbol{D}$ are the stress, the velocity, the pressure, the identity tensor, the viscosity, and the rate-of-deformation tensor, respectively, of the fluid.

2.2. Solid domain

The set of equations in the solid domain is given by the linearized elasticity (Hughes, 2000):

$$\nabla \cdot \boldsymbol{\sigma}_s = 0 \quad in\ P, \tag{4}$$

$$\nabla \cdot \boldsymbol{u}_s = 0 \quad in\ P, \tag{5}$$

$$\boldsymbol{\sigma}_s = -p_s \boldsymbol{I} + 2\mu \boldsymbol{\varepsilon}(\boldsymbol{u}_s) \quad \text{in } P. \tag{6}$$

Eqs. (4)-(6) are for the momentum balance, the continuity, and the constitutive relation, respectively, in the solid domain. The symbols $\boldsymbol{\sigma}_s$, $\boldsymbol{u}_s$, p_s, μ, and $\boldsymbol{\varepsilon}$ are the stress, the displacement, the pressure, the Lamé constant, and the (infinitesimal) strain tensor, respectively, of the solid. The incompressibility of solid is necessary in solid/fluid interaction problems, if the Dirichlet type boundary condition is applied for all domain boundaries. In this case, the Poisson ratio is 0.5 and then the Lamé constant in Eq. (6) is a multiple of Young's modulus E:

$$\mu = \frac{E}{2(1+\nu)} = \frac{1}{3}E. \tag{7}$$

2.3. Solid/fluid interaction

The force balance and the kinematic continuity condition around the solid boundary can be given by:

$$\boldsymbol{\sigma}_f \cdot \boldsymbol{n} = \boldsymbol{\sigma}_s \cdot \boldsymbol{n} \quad \text{on } \partial P, \tag{8}$$

$$\boldsymbol{v}_f = \frac{\boldsymbol{u}_s}{\Delta t} \quad \text{on } \partial P. \tag{9}$$

In Eqs. (8) and (9), $\boldsymbol{n}$ is the outward normal vector on the solid boundary from the solid body, and Δt is a pseudo-time step for connecting the fluid velocity and the solid displacement. In the weak formulation of the finite element method, the kinematic constraint is usually combined with the Lagrangian multiplier and the force balance is then satisfied implicitly through the multiplier. In this regard, we use the no-slip constraint (Eq. (9)) only in the derivation of the weak form.

3. Numerical methods

3.1. Combined weak formulation

We define the combined solution and variational spaces for the fluid velocity and the solid displacement as follows:

$$W_v = \left\{ (\boldsymbol{v}_f, \boldsymbol{u}_s) \,|\, \boldsymbol{v}_f \in H^1(\Omega \backslash P), \boldsymbol{u}_s \in H^1(P), \boldsymbol{v}_f = \frac{\boldsymbol{u}_s}{\Delta t} \text{ on } \partial P \right\}, \tag{10}$$

$$w_0 = \left\{ (\boldsymbol{w}_f, \boldsymbol{w}_s) | \boldsymbol{w}_f \in H^1(\Omega \backslash P), \boldsymbol{w}_s \in H^1(P), \boldsymbol{w}_f = \frac{\boldsymbol{w}_s}{\Delta t} \text{ on } \partial P \right\}. \quad (11)$$

The solution space for the fluid and solid pressure are $L^2(\Omega \backslash P)$ and $L^2(P)$, respectively. The combined weak formulation for the whole domain can be written as:

$$\int_{\Omega \backslash P} (\nabla \cdot \boldsymbol{\sigma}_f) \cdot \boldsymbol{w}_f d\Omega + \int_P (\nabla \cdot \boldsymbol{\sigma}_s) \cdot \frac{\boldsymbol{w}_s}{\Delta t} d\Omega = 0. \quad (12)$$

Integrating the stress-divergence terms by parts, one gets:

$$\int_{\Omega \backslash P} \boldsymbol{\sigma}_f : (\nabla \boldsymbol{w}_f) d\Omega + \frac{1}{\Delta t} \int_P \boldsymbol{\sigma}_s : (\nabla \boldsymbol{w}_s) d\Omega - \left[\int_{\partial P} (\boldsymbol{n}_f \cdot \boldsymbol{\sigma}_f) \cdot \boldsymbol{w}_f d\Gamma + \int_{\partial P} (\boldsymbol{n}_s \cdot \boldsymbol{\sigma}_s) \cdot \frac{\boldsymbol{w}_s}{\Delta t} d\Gamma \right] = 0. \quad (13)$$

The last two line integrals in Eq. (13) are canceled by Eqs. (8) and (9) so that the final combined weak formulation is as follows:

$$\int_{\Omega \backslash P} \boldsymbol{\sigma}_f : (\nabla \boldsymbol{w}_f) d\Omega + \frac{1}{\Delta t} \int_P \boldsymbol{\sigma}_s : (\nabla \boldsymbol{w}_s) d\Omega = 0. \quad (14)$$

We remark that the hydrodynamic force on the solid boundary is canceled in combined momentum equation (Eq. (14)). The weak formulation of the continuity equation for fluid and solid are as follows:

$$\int_{\Omega} (\nabla \cdot \boldsymbol{v}_f) q_f d\Omega = 0, \quad (15)$$

$$\int_P (\nabla \cdot \boldsymbol{u}_s) q_s d\Omega = 0. \quad (16)$$

3.2. DLM/FD weak formulation

By applying the fictitious domain (FD) concept, we extend the fluid domain ($\Omega \backslash P$) to the entire computational domain (Ω). Extending the no-slip constraint on the solid boundary to the interior of the solid domain, one gets:

$$\int_P \boldsymbol{\sigma}_f : \nabla \left(\boldsymbol{w}_f - \frac{\boldsymbol{w}_s}{\Delta t} \right) d\Omega = 0. \quad (17)$$

By applying Eq. (17) to Eq. (14), the FD weak formulation is presented as follows:

$$\int_{\Omega} \boldsymbol{\sigma}_f : (\nabla \boldsymbol{w}_f) d\Omega + \frac{1}{\Delta t} \int_P (\boldsymbol{\sigma}_s - \boldsymbol{\sigma}_f) : (\nabla \boldsymbol{w}_s) d\Omega = 0. \quad (18)$$

Now we introduce the Lagrangian multiplier, $\lambda \in L^2(P)$, on the solid domain to combine the no-slip constraint on the solid boundary (*or* over the solid domain). By using the Lagrangian multiplier, one gets the distributed-Lagrangian-multiplier/fictitious-domain (DLM/FD) weak formulation as follows:

$$\int_{\Omega} \boldsymbol{\sigma}_f : (\nabla \boldsymbol{w}_f) d\Omega + \int_{\partial P} \lambda \cdot \boldsymbol{w}_f d\Gamma = 0, \quad (19)$$

$$\int_{\Omega} (\nabla \cdot \boldsymbol{v}_f) q_f d\Omega = 0, \quad (20)$$

$$\frac{1}{\Delta t} \int_P (\boldsymbol{\sigma}_s - \boldsymbol{\sigma}_f) : (\nabla \boldsymbol{w}_s) d\Omega - \frac{1}{\Delta t} \int_{\partial P} \lambda \cdot w_s d\Gamma = 0, \quad (21)$$

$$\int_P (\nabla \cdot \boldsymbol{u}_s) q_s d\Omega = 0, \quad (22)$$

$$\int_{\partial P} \mu \cdot \left(\boldsymbol{v}_f - \frac{\boldsymbol{u}_s}{\Delta t} \right) d\Gamma = 0. \quad (23)$$

Note that the line integrals in Eqs. (19), (21), and (23) can be changed to domain integrals when the no-slip constraint is applied on the entire solid domain. For example, the last term in Eq. (19) can be changed to:

$$\int_P (\lambda \cdot \boldsymbol{w}_f) d\Omega.$$

3.3. Application to Newtonian fluid and Hookean solid

Now we consider the Newtonian constitutive equation for the fluid and the Hookean constitutive equation for the solid. Applying Eqs. (3) and (6) to Eqs. (19) and (21), one gets the formulation for the Newtonian fluid and the Hookean solid. As a result, the weak form for the whole domain can be stated as follows:

Find $\boldsymbol{v}_f \in H^1(\Omega)^2$, $\boldsymbol{u}_s \in H^1(P)^2$, $p_f \in L^2(\Omega)$, $p_s \in L^2(P)$ and $\lambda \in L^2(P)$ such that

$$-\int_{\Omega} p_f (\nabla \cdot \boldsymbol{w}_f) d\Omega + 2\eta \int_{\Omega} \boldsymbol{D}(\boldsymbol{v}_f) : \boldsymbol{D}(\boldsymbol{w}_f) d\Omega + \int_{\partial P} \lambda \cdot \boldsymbol{w}_f d\Gamma = 0, \quad (24)$$

$$\int_{\Omega} (\nabla \cdot \boldsymbol{v}_f) q_f d\Omega = 0, \quad (25)$$

$$-\int_P p_s (\nabla \cdot \boldsymbol{w}_s) d\Omega + 2\mu \int_P \boldsymbol{\varepsilon}(\boldsymbol{u}_s) : \boldsymbol{\varepsilon}(\boldsymbol{w}_s) d\Omega$$

$$-\left[-\int_P p_f (\nabla \cdot \boldsymbol{w}_s) d\Omega + 2\eta \int_P \boldsymbol{D}(\boldsymbol{v}_f) : \boldsymbol{\varepsilon}(\boldsymbol{w}_s) d\Omega \right] - \int_{\partial P} \lambda \cdot \boldsymbol{w}_s d\Gamma = 0, \quad (26)$$

$$\int_P (\nabla \cdot \boldsymbol{u}_s) q_s d\Omega = 0, \quad (27)$$

$$\int_{\partial P} \mu \cdot \left(\boldsymbol{v}_f - \frac{\boldsymbol{u}_s}{\Delta t} \right) d\Gamma = 0, \quad (28)$$

for all $\boldsymbol{w}_f \in H^1(\Omega)^2$, $\boldsymbol{w}_s \in H^1(P)^2$, $q_f \in L^2(\Omega)$, $q_s \in L^2(P)$ and $\mu \in L^2(P)$.

4. Implementation

4.1. Spatial discretization

Two discretization schemes have been used for solid/fluid interaction problem. A regular rectangular discretization with the bi-quadratic interpolation of the velocity and the linear discontinuous interpolation for the pressure ($Q_2 - P_1^d$ element) is employed for the fluid domain. In the solid domain a regular rectangular discretization is also used but with the bi-linear interpolation of the displacement and the constant pressure element ($Q_1 - P_0$ element). To impose no-slip constraint on the solid boundary, we applied the distributed Lagrangian multiplier method. For the computational convenience, multipliers are imposed on every nodal point on the solid boundary (*or* on the solid

domain).

4.2. Matrix equation

Using the discretization mentioned above, one gets the following matrix equation at each time step for a given solid configuration:

$$\begin{bmatrix} K_f & G_f & 0 & 0 & N_f \\ G_f^{\mathrm{T}} & 0 & 0 & 0 & 0 \\ I & P & K_s & G_s & -N_s \\ 0 & 0 & G_s^{\mathrm{T}} & 0 & 0 \\ N_f^{\mathrm{T}} & 0 & -\frac{1}{\Delta t}N_s^{\mathrm{T}} & 0 & 0 \end{bmatrix} \begin{bmatrix} \boldsymbol{v}_f \\ -p_f \\ \boldsymbol{u}_s \\ -p_s \\ \lambda \end{bmatrix} = \boldsymbol{f}. \tag{29}$$

K_f, G_f, K_s, G_s represent sub-matrices for the fluid velocity, the incompressibility of the fluid, the solid displacement and the incompressibility of the solid, respectively. The no-slip constraint with the Lagrangian multiplier is denoted by sub-matrices N_f and N_s. The sub-matrices I and P account for the fluid stress inside the solid domain. The construction of I and P is not straight forward, since the evaluation of fluid stress at the solid element cannot be done with the conventional quadrature integral. In this regard, to access the necessity of the use of I and P, we performed numerical tests in section 5. In case of Yu (2005), the fluid stress in the solid domain has been neglected.

The asymmetric sparse matrix is solved by a direct method based on a sparse multifrontal variant of Gaussian elimination (HSL/MA41) (Amestoy and Duff, 1989; Amestoy and Duff, 1993; Amestoy and Puglisi, 2003).

4.3. Time integration

At each (pseudo) time step, the solid position changes and we need to modify the solid configuration and the stress. For a given initial solid configuration, one can construct and solve the matrix equation in Eq. (29). Then, from the solution of the previous time step, one can update the solid configuration and the stress. One needs several iterations to reach the steady state deformation. In this study, we use the convergence criteria (t_c) as follows:

$$t_c = \frac{|\boldsymbol{u}_s^t|}{|\boldsymbol{u}_s^0|} \le 10^{-5}, \tag{30}$$

where $\boldsymbol{u}_s^0$ is the displacement of the first iterate and $\boldsymbol{u}_s^t$ is the displacement at pseudo-time step t.

5. Results

5.1. Numerical experiment

We consider an elastic solid bar attached on the bottom in a pressure-driven channel flow of a Newtonian fluid as shown in Fig. 1. The height of the solid bar is a half of the channel height, and the width of the solid bar is 1/5 of the channel length. The computational domain is from (0, 0) to (1, 1) and the bottom center of the solid bar is located at (0.5, 0). The bottom of the solid domain is pinned by the boundary condition. For the fluid domain, the no-slip boundary condition is imposed on Γ_2 and Γ_4, and traction boundary condition is imposed on Γ_1 and Γ_3 to generate the pressure difference. To investigate the effect of the distribution of Lagrangian multipliers, we compared the results of the Lagrangian multipliers over the entire solid domain (D) with those of the Lagrangian multipliers on the solid boundary only (B). Also, to assess the necessity of considering fluid stress in the solid domain, we denote a problem with sub-matrices I and P by SV and a problem without I and P by V. The four sets, two different conditions for each factor, have been listed in Table 1. To understand the effect of each factor and to find the optimum condition, we performed numerical experiments for the four sets and checked the mesh convergence and the pseudo-time step dependence to evaluate the robustness of the present formulation. The results are presented from all four sets together for the proper comparison.

Table 1. Four different sets for numerical experiments

	Distribution of Lagrangian multipliers	Solid/fluid interfacial condition
B_V	on the solid boundary	w/o fluid stress inside the solid
D_V	over the solid domain	w/o fluid stress inside the solid
D_SV	over the solid domain	with fluid stress inside the solid
B_SV	on the solid boundary	with fluid stress inside the solid

5.2. Mesh convergence

We performed the mesh refinement test, using five different meshes: a 20-by-20 fluid mesh with a 2-by-10 solid mesh, denoted by F(400)/S(20), to a 60-by-60 fluid mesh with 6-by-30 solid mesh, denoted by F(3600)/S(180). All five meshes have the same mesh size ratio between solid mesh and fluid mesh. The solid displacements, $du_s = \sqrt{(u_{s,x})^2 + (u_{s,y})^2}$, along the left side of the solid bar, the displacement from bottom-left ($y=0$) to top-left point ($y=1$) of the solid bar, are presented in Fig. 2. As shown in Fig. 2, all four sets show good mesh convergence. The mesh convergence is also confirmed in the prediction of solid strains ε_{11} (Fig. 3) and ε_{22} (Fig. 4). Next, we assigned a larger pressure gradient by the factor of 10 and investigated mesh convergence. As shown in Fig. 5, the result shows good mesh convergence, even though the solid displacement appears much larger than before (but still within

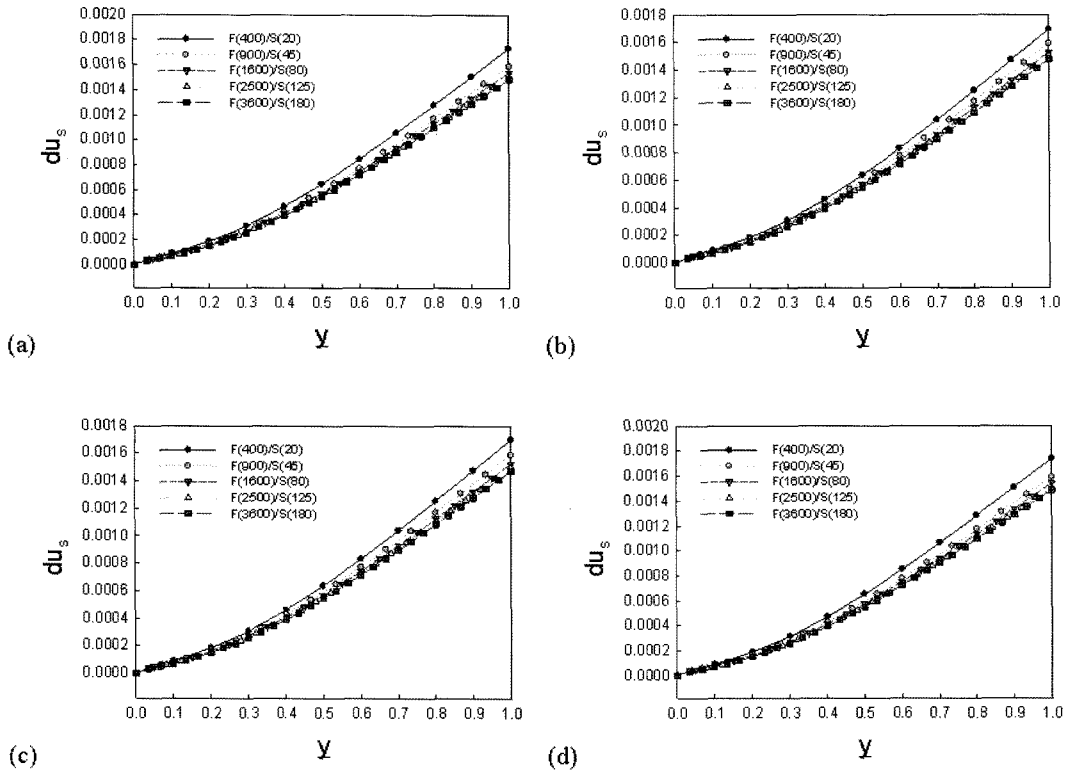

Fig. 2. Mesh convergence: comparison of the solid displacement at $\Delta p=1$, $E=10^5$, $\nu=0.5$, $\Delta t=0.001$. (a) B_V, (b) D_V, (c) D_SV, (d) B_SV.

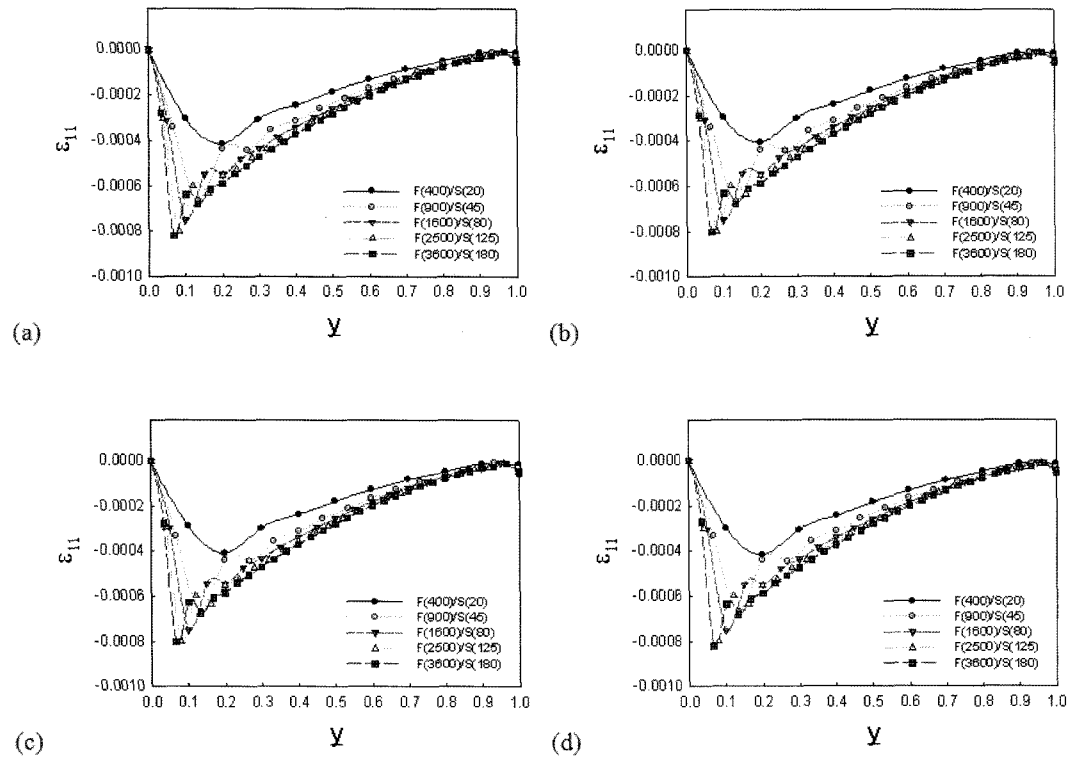

Fig. 3. Mesh convergence: comparison of the solid strain (ε_{11}) at $\Delta p=1$, $E=10^5$, $\nu=0.5$, $\Delta t=0.001$. (a) B_V, (b) D_V, (c) D_SV, (d) B_SV.

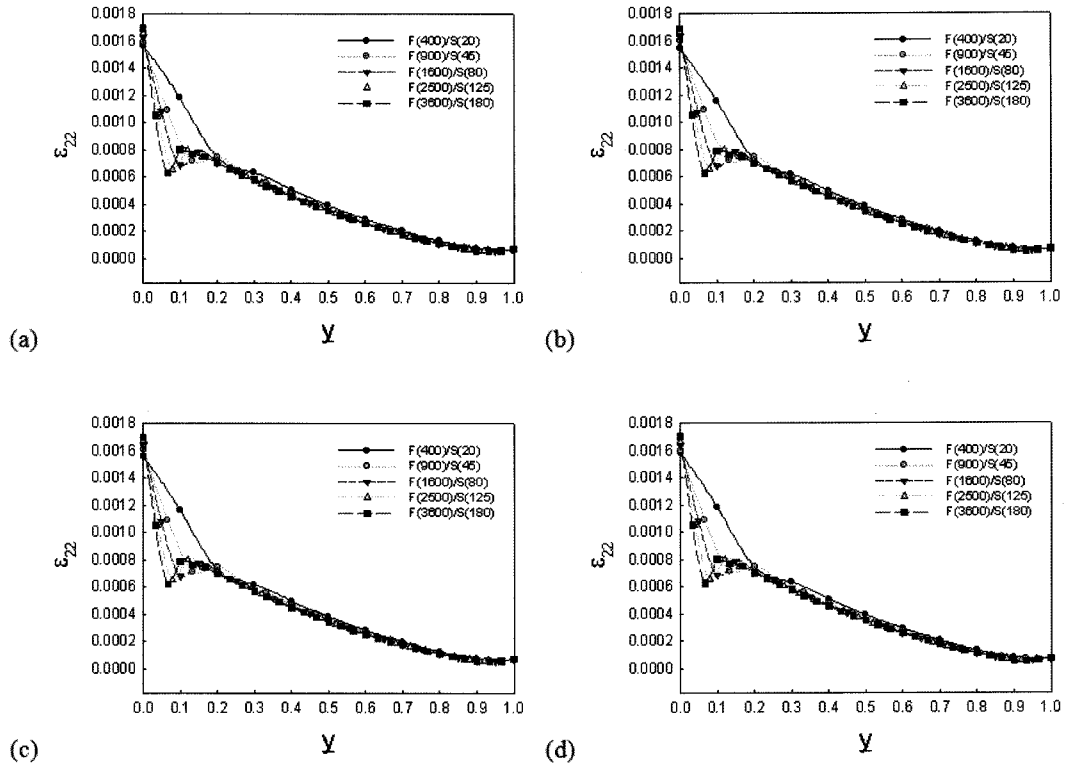

Fig. 4. Mesh convergence: comparison of the solid strain (ε_{22}) at $\Delta p=1$, $E=10^5$, $\nu=0.5$, $\Delta t=0.001$. (a) B_V, (b) D_V, (c) D_SV, (d) B_SV.

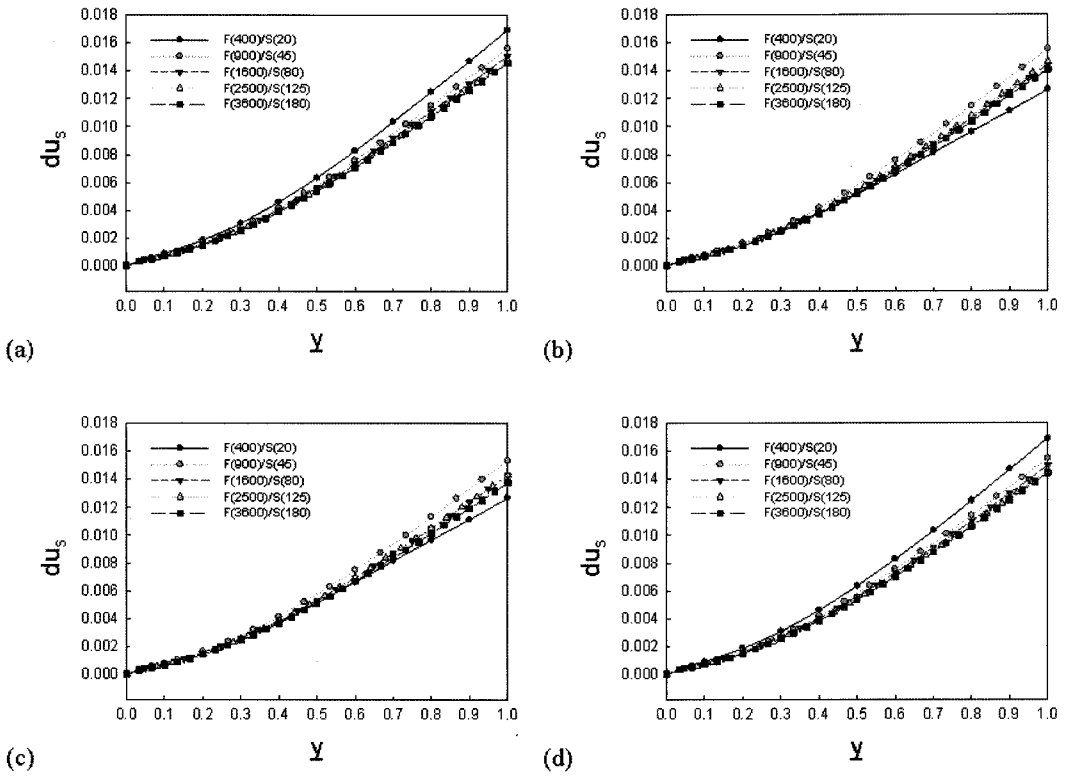

Fig. 5. Mesh convergence: comparison of the solid displacement at $\Delta p=10$, $E=10^5$, $\nu=0.5$, $\Delta t=0.001$. (a) B_V, (b) D_V, (c) D_SV, (d) B_SV.

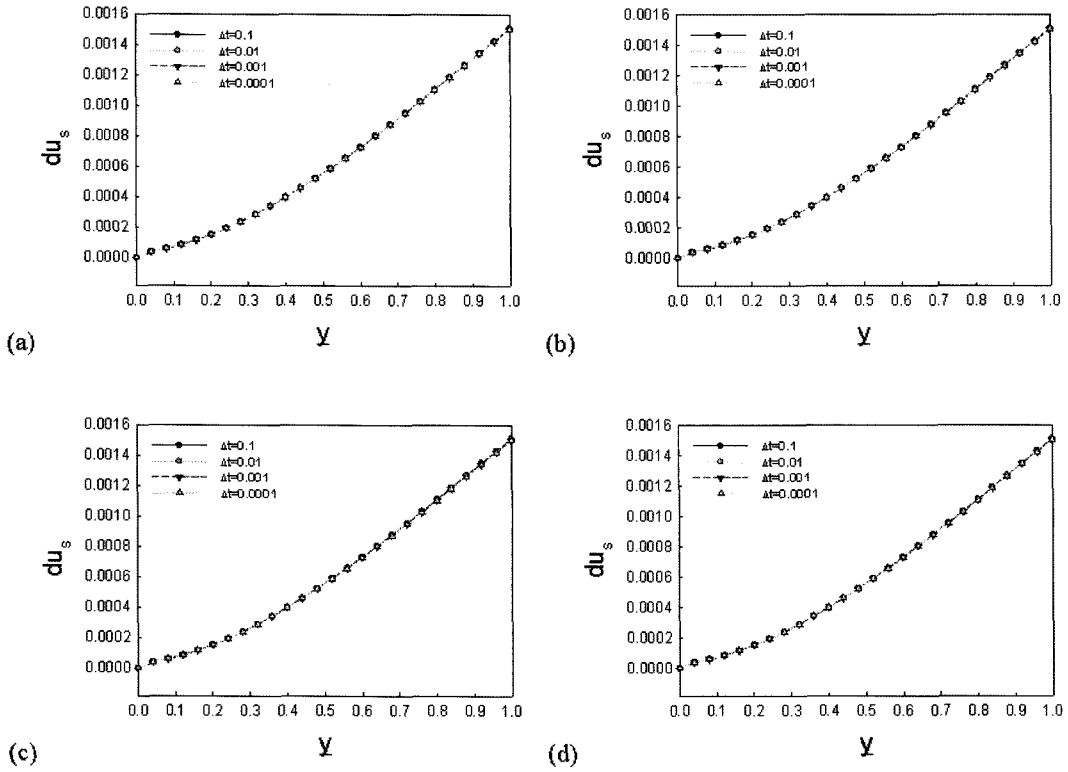

Fig. 6. Pseudo-time step dependence: comparison of the solid displacement at $\Delta p=1$, $E=10^5$, $\nu=0.5$ with F(2500)/S(125) mesh set. (a) B_V, (b) D_V, (c) D_SV, (d) B_SV.

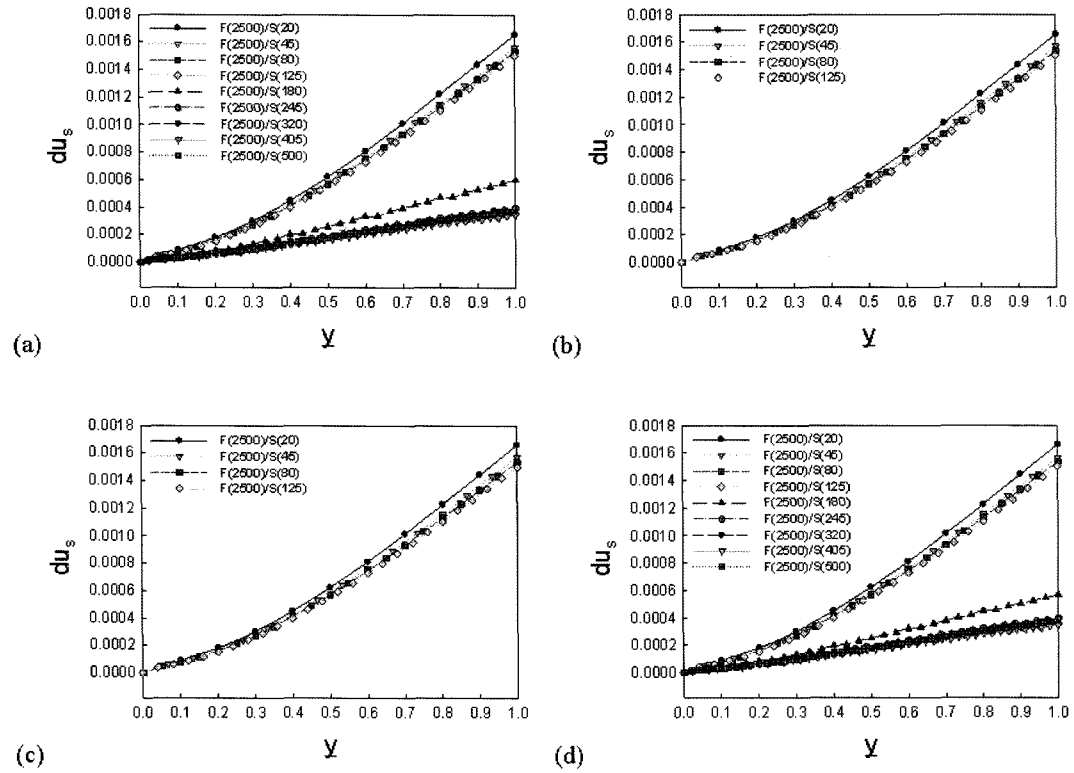

Fig. 7. Solid/fluid mesh ratio: comparison of the solid displacement at $\Delta p=1$, $E=10^5$, $\nu=0.5$, $\Delta t=0.001$ with fixed fluid mesh as F(2500). (a) B_V, (b) D_V, (c) D_SV, (d) B_SV.

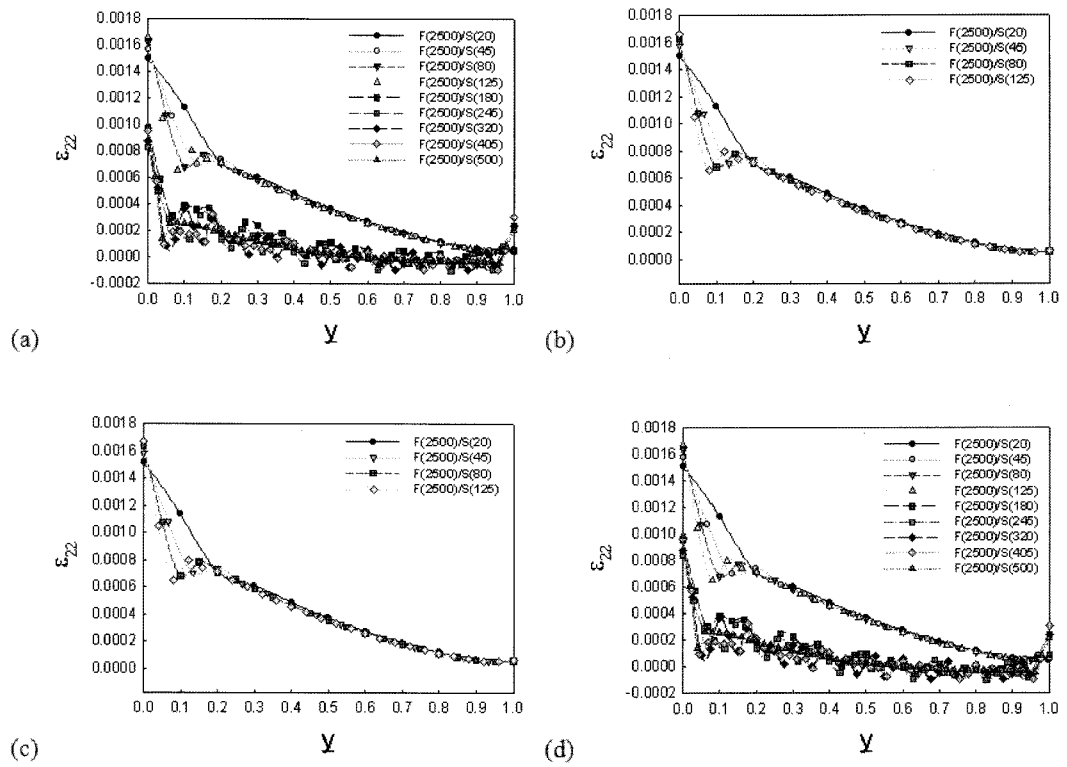

Fig. 8. Solid/fluid mesh ratio: comparison of the solid strain (ε_{22}) at $\Delta p=1$, $E=10^5$, $\nu=0.5$, $\Delta t=0.001$ with fixed fluid mesh as F(2500). (a) B_V, (b) D_V, (c) D_SV, (d) B_SV.

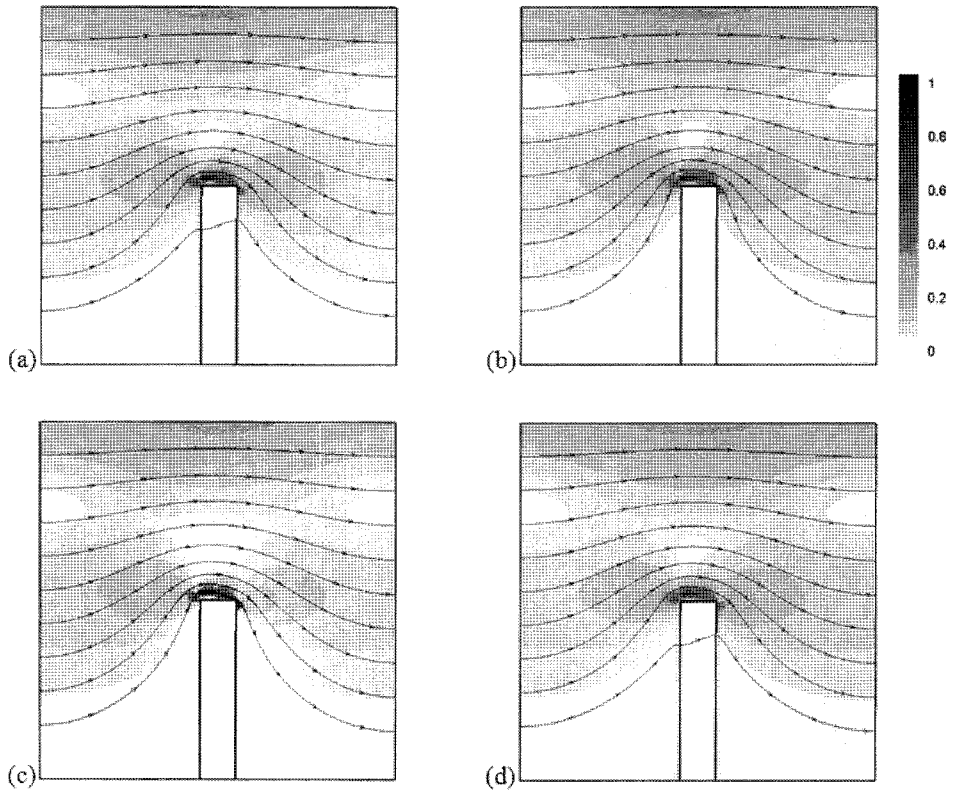

Fig. 9. The distribution of shear rate and the streamline: comparison of the results at $\Delta p=1$, $E=10^5$, $\nu=0.5$, $\Delta t=0.001$ with fixed fluid mesh as F(2500)/S(125). (a) B_V, (b) D_V, (c) D_SV, (d) B_SV.

a linearized elasticity regime).

Interestingly, there is no significant difference among the four sets, which indicates that the influence of the fluid stress in the solid domain is very minor. Reminding that the treatment of the fluid stress inside the solid domain, *i.e.* construction of I and P sub-matrices, is a quite tedious process, as implied from the results, it may be possible to neglect this minor contribution.

5.3. Pseudo-time step dependence

To investigate the effect of pseudo-time stepping, we tested the pseudo-time step from 0.1 to 0.0001, while other conditions being fixed. Note that the pseudo-time step in Eq. (9) was adopted to connect the fluid velocity and the solid displacement, hence it is required that the results have a little dependence on this pseudo-time step. As shown in Fig. 6, there is almost no time step dependence. With this result, we can assure the robustness of the present algorithm. In addition, there is no significant difference among the four sets, which implies that it is possible to neglect the fluid stress inside the solid domain as mentioned before.

5.4. Solid/fluid mesh ratio

To find out the optimal solid/fluid mesh ratio, we change the number of elements from 20 (2-by-10) to 500 (10-by-50) for the solid mesh with fixed fluid mesh as 2500 (50-by-50) elements. Since use 9-node quadrilateral elements for the fluid and 4-node quadrilateral element for the solid, the solid and fluid have the same mesh size of the ratio 1 when the number of elements of the solid mesh is 125 (5-by-25). Note that the change of the solid mesh means the change of the number of collocation points since we applied Lagrangian multipliers on solid nodal points. The finer solid mesh, the more Lagrangian multipliers on the interface where the interfacial conditions are enforced. When the solid mesh size gets bigger than or comparable to the fluid mesh size, similar results are obtained as in Fig. 7 (the solid displacement) and Fig. 8 (the solid strain ε_{22} component). When the solid mesh size becomes smaller than the fluid mesh size, there appear locking problems with numerical errors, because of the excessive constraints inside the fluid element. Especially, the results show that this locking appears even worse, if the Lagrangian multipliers are distributed over the solid element. Conclusively, it would be good to use comparable or bigger solid meshes than the fluid mesh to avoid the locking problem.

5.5. Streamline and shear rate distribution

The streamline and shear rate distribution of the fluid with the final shape of the solid bar are shown together in Fig. 9. Here, the sets of D_V and D_SV in which Lagrangian multipliers are on the entire solid domain show smooth contours compared to the others. When Lagrangian multipliers are applied only on the solid boundary, one can observe the shear rate jump around the collocation points. When the larger pressure gradient is applied, the shear rate jump on the solid boundary is more serious if Lagrangian multipliers are applied just on the solid boundary. One can also observe velocity vectors passing through the solid boundary in this case. In case of the Lagrangian multipliers over the entire solid domain, one can see much smooth shear rate distribution. Conclusively, it seems to be better to apply the Lagrangian multipliers over the entire solid domain.

6. Conclusions

In this study, the distributed-Lagrangian-multiplier/fictitious-domain (DLM/FD) method has been applied to the elastic solid/Stokes flow interaction problem. The purpose of this numerical work is to find out the proper condition in using the DLM/FD scheme to the solid/fluid interaction problem. The robustness of this simulation algorithm has been verified through the mesh convergence and pseudo-time step dependence test. All four sets showed good mesh convergence, and there was no pseudo-time step dependence. We found that too many collocation points for the Lagrangian multipliers may cause a locking problem through the tests with different solid/fluid mesh sets. It is recommended to use comparable or bigger solid meshes compared to the size of the fluid mesh. We also found that consideration of the fluid stress inside the solid domain on the solid/fluid interface does not affect the results significantly. It has been found that the fluid stress in a fictitious solid domain may be neglected and the no-slip condition between the solid and fluid works since to be sufficient, which makes the algorithm much easier to be implemented. The dependency on the distribution of Lagrangian multipliers was also investigated: shear rate jump has been observed in case of the Lagrangian multipliers located only on the solid boundary. Conclusively, the fluid stress of the fictitious domain can be neglected and the Lagrangian multipliers need to be applied on the entire solid domain. Based on these results, we extend this algorithm to more challenging problems such as a freely suspended elastic particle in the Stokes flow, and systems of particles in a viscoelastic medium.

Acknowledgement

This work was supported by the National Research Laboratory Fund (M10300000159) of the Ministry of Science and Technology in Korea.

References

Allen, M. P. and D. J. Tildesley, 1987, Computer Simulation of Liquids, Oxford University Press, Oxford, UK.

Amestoy, P. R. and I. S. Duff, 1989, Vectorization of a Multiprocessor Multifrontal Code, *Intern. J. Supercomput. Applicat.* **3**(3), 41-59.

Amestoy, P. R. and I. S. Duff, 1993, Memory Management Issues in Sparse Multifrontal Methods on Multiprocessors, *Intern. J. Supercomput. Applicat.* **7**(1), 64-82.

Amestoy, P. R. and C. Puglisi, 2003, An unsymmetrized multifrontal LU factorization, *SIAM J. Matrix Anal. Applicat.* **24**(2), 553-569.

Baaijens, F. P. T., 2001, A fictitious domain/mortar element method for fluid-structure interaction, *Int. J. Numer. Methods Fluids* **35**(7), 743-761.

Donea, J., S. Giuliani and J. P. Halleux, 1981, Arbitrary Lagrangian-Eulerian finite element method for transient dynamic fluid-structure interactions, *Comput. Methods Appl. Mech. Eng.* **33**(1-3), 689-723.

Glowinski, R., T. W. Pan, T. I. Hesla and D. D. Joseph, 1999, A distributed Lagrange multiplier fictitious domain method for particulate flows, *Int. J. Multiph. Flow* **25**(5), 755-794.

Hu, H. H., 1996, Direct simulation of flows of solid-liquid mixtures, *Int. J. Multiph. Flow* **22**(2), 335-352.

Hughes, T. J. R., 2000, The Finite Element Method: linear static and dynamic finite element analysis, Dover publications, New York, US.

Hütter, M., 1999, Brownian Dynamics Simulation of Stable and of Coagulating Colloids in Aqueous Suspension, PhD Thesis, ETH, ZURICH.

Hwang, W. R., M. A. Hulsen and H. E. H. Meijer, 2004, Direct simulation of particle suspensions in sliding bi-periodic frames, *J. Comput. Phys.* **194**(2), 742-772.

Laso, M. and H. C. Öttinger, 1993, Calculation of Viscoelastic Flow Using Molecular-Models - the Connffessit Approach, *J. Non-Newtonian Fluid Mech.* **47**, 1-20.

Trofimov, S. Y., 2003, Thermodynamic consistency in dissipative particle dynamics, PhD Thesis, Technische Universiteit Eindhoven, Eindhoven.

Yu, Z., 2005, A DLM/FD method for fluid/flexible-body interactions, *J. Comput. Phys.* **207**(1), 1-27.